Materials Research Proceedings 41 (2024) 1017-1026 https://doi.org/10.21741/9781644903131-112

Evaluation of correlations between principal axes in uniaxial tensile tests of aluminum based on Mohr's strain circle

IIZUKA Takashi[1,a *]

[1]Faculty of Mechanical Engineering, Kyoto Institute of Technology, Matsugasaki Goshokaido-cho, Sakyo-ku, Kyoto 606-8585, Japan

[a]tiizuka@kit.ac.jp

Keywords: Anisotropic Metals, Principal Axes, The Associated Flow Rule, Mohr'S Strain Circle

Abstract. Anisotropic elasticity is expected to contribute significantly to material deformation and should be considered in nature. Therefore, in this study, the correlations between elastic and plastic strains are investigated, with emphasis on the principal axes. In an experiment, strains are measured in eight directions during tensile tests, and Mohr's circles are derived for elastic and plastic strains. The planar anisotropy of elasticity and plasticity for some mechanical properties is confirmed, and the angle deviations between the principal axes of stress and strain are compared for elasticity and plasticity. In the case of aluminum, for both elasticity and plasticity, the planar anisotropy of its mechanical properties indicates four-fold symmetry, and the principal axes of elastic and plastic strains are identical, with some angle deviations from the principal axes of stress.

Introduction

The fundamental theory of plasticity is applicable to isotropic materials and is summarized based on the Mises' yield criterion and the associated flow rule. The von Mises yield criterion presents a yield surface with a circular cylinder shape in the principal stress field; however, Bishop and Hill indicated that yield criteria that present pillar-type surfaces with a cross-section of six-fold symmetry may be suitable for isotropic materials if the Bauschinger effect is disregarded [1]. This implies that all yield functions for isotropic materials can be expressed by those proposed by Hosfold [2].

Hill first proposed a theory of plasticity for anisotropic materials in 1948 [3]. The criterion is extremely simple and easy to adopt for numerical simulations; however, it presents several drawbacks, such as the inability to express the yield stress and Lanford value simultaneously. After the introduction of the theory above, the anisotropy of yield surfaces in the principal stress field was discussed extensively; however, substantial new proposals regarding the yield criterion for anisotropic materials did not appear until the work of Barlat et al. in 1991 [4]. Barlat et al. developed a criterion in a step-by-step manner and presented a substantial final version in 2003 [5-7]. This yield criterion is extremely flexible and is considered the best for expressing the yielding of anisotropic materials.

Additionally, the plasticity of anisotropic materials has been investigated based on crystal plasticity. Bishop and Hill derived anisotropic yield surfaces by considering the plastic deformation of crystal grains in polycrystalline aggregates [1, 8]. Such attempts to obtain a yield surface based on crystal plasticity were similarly performed by Hutchinson, and Logan and Hosforld [9, 10]; however, the method to obtain the yield surface is extremely complicated and thus not applicable to general-purpose numerical simulations, such as finite-element analysis. Meanwhile, Asaro established a crystal-plasticity method that incorporated inclusions and self-consistent using the finite-element method (FEM) [11]. This method is extremely useful and widely used; however, the isotropic elasticity was initially assumed even in CP-FEMs. In recent years, the anisotropic elasticity has been considered in most studies using CP-FEM. However, the

effect of anisotropic elasticity obtained from such simulations have not been reflected in macroscopic yield functions.

Therefore, in this study, macroscopic correlations between elastic and plastic strains are investigated, with emphasis on the principal axes. Tensile tests are conducted to measure the strains in eight directions, and the development of Mohr's circles for elastic and plastic strains is investigated. Some elastic and plastic properties are confirmed, and the angle deviations between the principal axes of stress and strain are compared for elastic and plastic cases.

Measurement of strain in multiple directions

In this study, eight strain gauges were used to measure Mohr's strain circle via a uniaxial tensile test. The strain gauges were fixed every 22.5°, and the angle of direction for each strain gauge from the tensile direction was termed the measuring direction θ. This indicates that the angular distribution of the normal strain is measured from 0° to 157.5° during the tensile test. The JIS No.5 standard tensile specimen configuration was adopted, and the positions for fixing the strain gauges were determined based on a base point, which was the center point of the tensile specimen, as shown in Fig. 1.

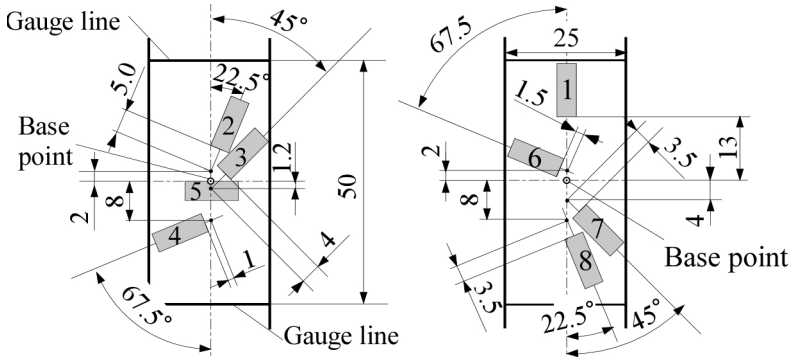

Figure 1 Fixing configuration of eight strain gauges.

Pure aluminum (JIS A1050P-O) with a thickness of 1 mm was used. Tensile tests were conducted by varying the tensile direction every 15° from the rolling direction, and this direction was defined as the tensile direction ϕ, as shown in Fig. 2(a). A Cu-Ni-type strain gauge with a gauge length of 5 mm (Tokyo Measuring Instruments Laboratory, YEFLAB-5) was used to measure the strain in the plastic-deformation region. A strain of approximately 10% can be measured using this strain gauge. In such strain measurements, material rotation is assumed to

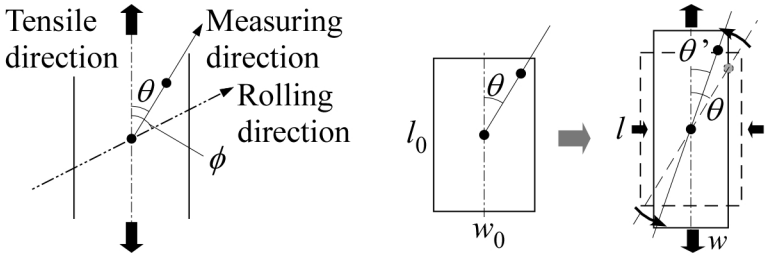

(a) Geometrical parameters (b) Rotation in measuring direction

Figure 2 Geometrical parameters and material rotation in uniaxial tensile test.

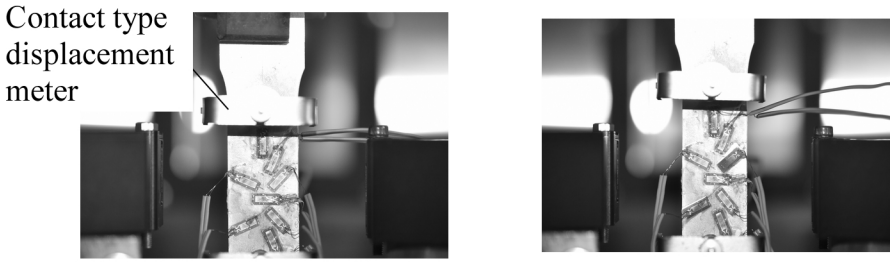

(a) Stroke 0 mm (b) Stroke 12 mm

Figure 3 Appearance of tensile test based on eight strain gauges.

occur continuously with increasing plastic elongation. Because the material rotation is assumed to be caused by plastic deformation, the ideal variation in each measurement direction was calculated from the measured plastic strain in both the tensile and transverse directions, as shown in Fig. 2(b). The appearance of a tensile specimen before and during the tensile test is shown in Fig. 3. The occurrence and extent of the material rotation can be confirmed from this figure. In the Results section, the first effect of this material rotation is shown.

Incremental uniaxial tensile test

To measure the elastic and plastic strains concurrently, a uniaxial tensile test was conducted by incrementally adding plastic strain. An example of a tensile load–stroke diagram is shown in Fig. 4(a). The initial distance between the chucks was set to 100 mm, and loading and unloading were repeated after adding the displacement prescribed in advance as a stroke between the chucks. As shown in Fig. 4(a), the displacement was prescribed to be smaller in the early stage, and it was increased with respect to a plastic elongation. The additional stroke was 0.12 mm when the stroke between the chucks, u, was 0–1.2 mm, and it was increased to 0.24 and 0.60 mm until the stroke reached 2.4 and 6.0 mm, respectively. Although the results for further loading are also shown in the figure, the discussion herein is based on only the results obtained for strokes from 0 to 6.0 mm.

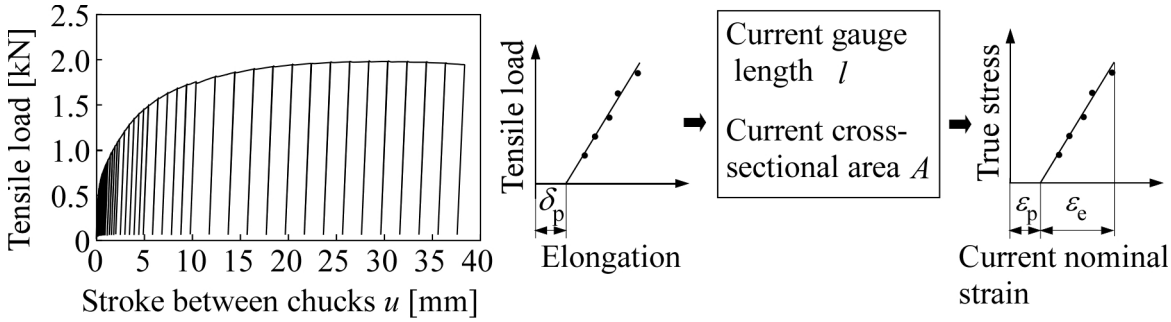

(a) Incremental uni-axial tensile test (b) Calculation of current nominal strain

Figure 4 Uniaxial tensile test and evaluation of stress and strain.

In the measurement, a contact-type displacement meter was used together, and the displacement between gauge lengths of 50 mm was measured more precisely. As shown in Fig. 4(b), because some plastic elongation, δ_p, appeared after each unloading, the current cross-sectional area, A, was estimated from the current gauge length, l, based on the volume constancy law. The true stress was calculated using the current cross-sectional area, and the elastic strains measured by the strain gauges were re-evaluated by considering the plastic strain given by that time. The relationship between the true stress, σ, and elastic strain in each measuring direction, $\varepsilon_e(\theta)$, can be approximated as a linear function, as follows:

$$\sigma = E(\theta)\varepsilon_{\mathrm{e}}(\theta), \tag{1}$$

where E is the linear coefficient in each direction; notably, this coefficient is no longer a component of the elastic modulus tensor or matrix. Meanwhile, the inverse of coefficient C is related to the component of the elastic compliance tensor or matrix. Because the value of the true stress is the one in tensile direction and common in every θ,

$$\frac{\varepsilon_{\mathrm{e}}(\theta)}{\sigma} = C(\theta) \tag{2}$$

is obtained by dividing the measured elastic strain by the true stress, which can be used as an elastic variable instead of the elastic strain. When linear elastic theory is assumed, this elastic variable is not affected directly by the amount of elastic strain; thus, it can be used conveniently for examining elastic properties. In addition, it can be correlated with the elastic compliances, such as

$$C(0°)=C_{11}(\phi), \quad C(90°)=C_{12}(\phi), \tag{3}$$

where C_{11} and C_{12} are the components of the elastic compliance matrix, denoted by the Voigt notation. The plastic strain in each direction was calculated as the logarithmic strain from the strain measured using strain gauge after unloading.

Estimation of Mohr's strain circle

Based on the elastic and plastic strains measured in the measuring directions, each Mohr's strain circle was estimated, and the elastic/plastic properties and angle deviation of the principal strain direction from tensile direction, ψ, was calculated. The Mohr's circle was estimated using two different methods: the least-squares approximation (LSA) and the discrete Fourier transformation (DFT). Using the LSA, the coefficient of determination,

$$R^2 = \frac{\sum_{i}^{n}(y_i - f(x_i))^2}{\sum_{i}^{n}(y_i - \overline{y}_i)^2}, \tag{4}$$

was used to determine the diameter and center coordinates of the circle and the angle deviation. In the equation above, x_{i} and y_{i} are the experimental values, and $f(x)$ and $\overline{y}_i$ are the approximated linear function and average value of y_{i}, respectively. If the angle deviation is provided, then the normal strain is expressed as a first-order function of $\cos 2(\theta - \psi)$; hence, the intercept and coefficient can be decided based on LSA. The intercept is the center coordinate of the normal strain, and the coefficient is the radius of the circle. The R^2 was calculated by varying the angle deviation from -45° to 45°, and the angle deviation with the largest R^2 was adopted.

Meanwhile, using the DFT, terms other than the constant and a period of 180° were disregarded after frequency resolution. The value of the constant term is the center coordinate of the normal strain, and the coefficient of the term with a period of 180° is the radius of the circle. The angle deviation was calculated by synthesizing sine and cosine functions. However, the DFT method is intrinsically valid only for data with a constant angle interval.

Materials Research Proceedings 41 (2024) 1017-1026 https://doi.org/10.21741/9781644903131-112

Material rotation in uniaxial tensile test

As mentioned previously, the measurement directions of strain were rotated by plastic deformation. Therefore, the effect of material rotation on strain measurement was investigated. The direction of each strain gauge was measured from photographs captured after each unloading process using graphics software. As an example, variations with stroke in the direction of eight strain gauges for $\phi = 0°$ is shown in Fig. 5. In this figure, the curves drawn for each direction were approximated from those estimated using the volume constancy law. However, the angles were measured by assuming the vertical direction on the photograph as the tensile direction. As shown in the figure, each measurement direction varied slightly, whereas the rotation minimally affected the strain measurement. The maximum rotation was 3°, and the variation was reflected in the LSA. In the DFT approximation, this variation was disregarded.

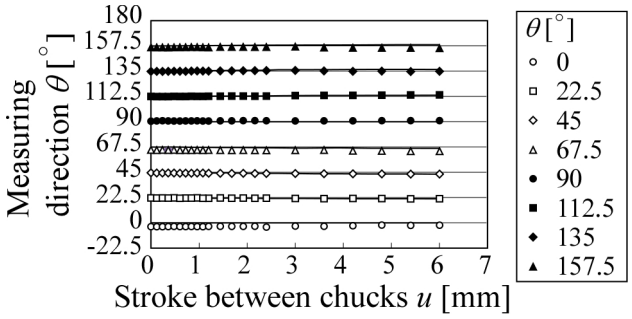

Figure 5 Variations in measuring direction with uniaxial tension (ϕ=0°).

Elastic properties and deviation between principal axes of stress and strain

Fig. 6 shows the variations in the elastic variables defined in Eq. 2 for measuring the direction from 0° to 157.5° under $\phi = 30°$ with increasing stroke between chucks. As shown in this figure, the variables increase significantly in the early stage; however, the variation became almost linear and moderate beginning from $u = 1$ mm.

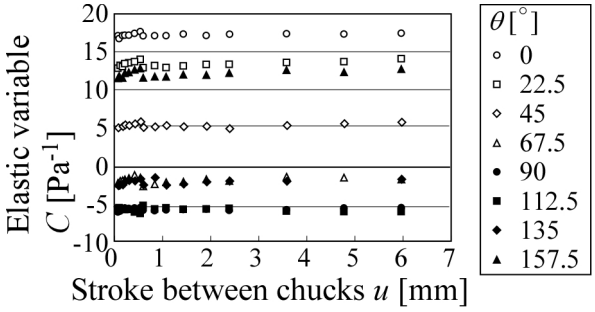

Figure 6 Variations in elastic variable C for incremental uniaxial tension (ϕ = 30°).

Variations in the linear coefficient E and elastic variable C with the measuring direction are shown for the case of $\phi = 30°$ in Fig. 7. In this figure, the variations at $u = 0.6$, 1.2, and 2.4 mm are compared. As shown in Fig. 6, almost no differences were observed between the strokes in both cases. For the linear coefficient E, no clear relationships were indicated, whereas for the elastic variable, clear cosine-like curves depicting the relationship between C and θ were expected. This implies that Mohr's strain circle can be estimated from these results for the elastic variable.

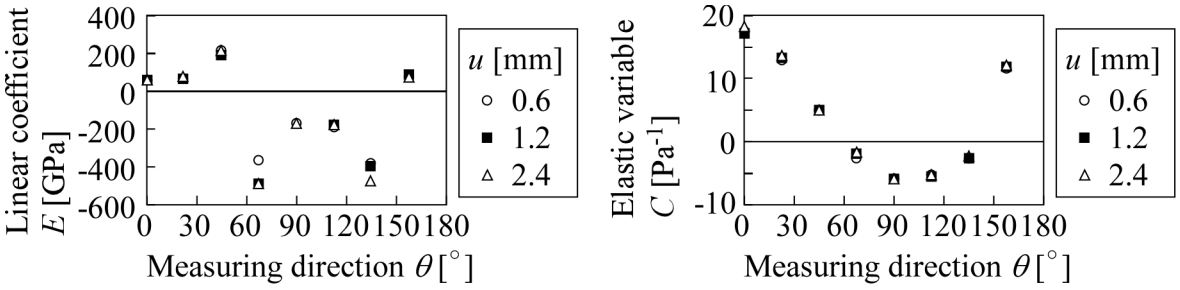

(a) Linear coefficient E (b) Elastic variable C

Figure 7 Variations in linear coefficient E and elastic compliance C with θ (ϕ =30°).

As mentioned previously, Mohr's circle was estimated using the LSA and DFT. The angular deviation between the principal axes of stress and strain can be obtained from these approximations as well. For the elastic strain, the anisotropy of the elastic properties can be discussed using C instead of using the elastic strain, as shown in Eq. 2. Furthermore, if $\theta = 0°$ and $\theta = 90°$ are adopted for the obtained Mohr's strain circle, then the elastic compliances C_{11} and C_{12} can be expressed as shown in Eq. 3, respectively.

As for the tensile direction $\phi = 75°$, variations in C_{11} and C_{12} and the angle deviation ψ with the stroke u are shown in Fig. 8. In this figure, only the results with a high R^2 exceeding 0.9 for the LSA are plotted, and the results obtained using the two approximations are compared. Fig. 8(a) shows that the value of C_{11} is approximately 15Pa^{-1}. The initial value of C_{11} was approximately 13 Pa^{-1}, which then increased nonlinearly and significantly until approximately u = 1 mm. When the stroke was greater than 1 mm, the increase diminished, and the value remained almost constant. The two approximation methods did not indicate any difference.

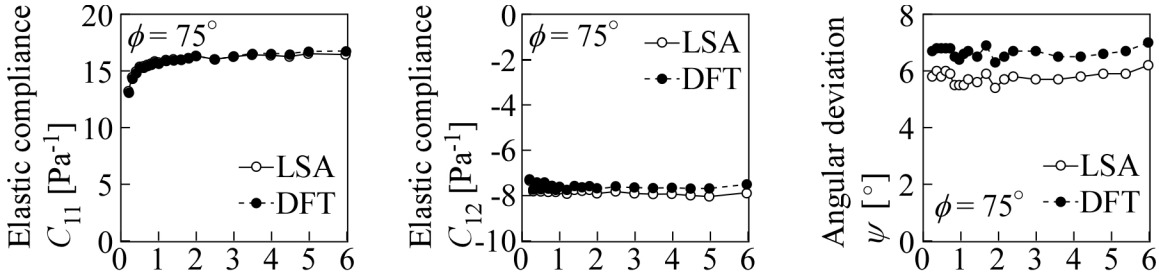

(a) C_{11} (b) C_{12} (c) Deviation angle ψ

Figure 8 Variations in elastic compliances C_{11} and C_{12}, and deviation angle ψ for ϕ =75°.

As shown in Fig. 8(b), variations in C_{12} with stroke were not observed in either approximation. The value of C_{12} was approximately -8 Pa^{-1} for both approximation methods. Meanwhile, the angle deviated by 6° to 7°. This deviation, although small in magnitude, had a significant meaning in mechanics. Thus, one can conclude that the principal axis of elastic strain no longer agreed with that of stress when the tensile direction was not the symmetric axis of the sheet metal. Variations in the angle deviation were not observed, even when the stroke increased. The DFT estimated a slightly larger deviation than the LSA; however, the results can be regarded are similar.

Next, the anisotropies of the elastic properties and angle deviation are shown for u = 1.2 mm in Fig. 9. In this figure, the horizontal axis represents the tensile direction, and the planar anisotropies estimated using the two approximations are compared. First, for elastic compliance C_{11} shown in Fig. 9(a), the planar anisotropy showed four-fold symmetry, as expected. C_{11} indicated a high value of approximately 16.5 Pa^{-1} at ϕ = 0° and ϕ = 90°, i.e., in the rolling and transverse directions,

respectively, and the lowest value of approximately 15 Pa^{-1}near $\phi = 45°$. This tendency was similar in the two approximations; however, the LSA estimated a slightly better ordered symmetry.

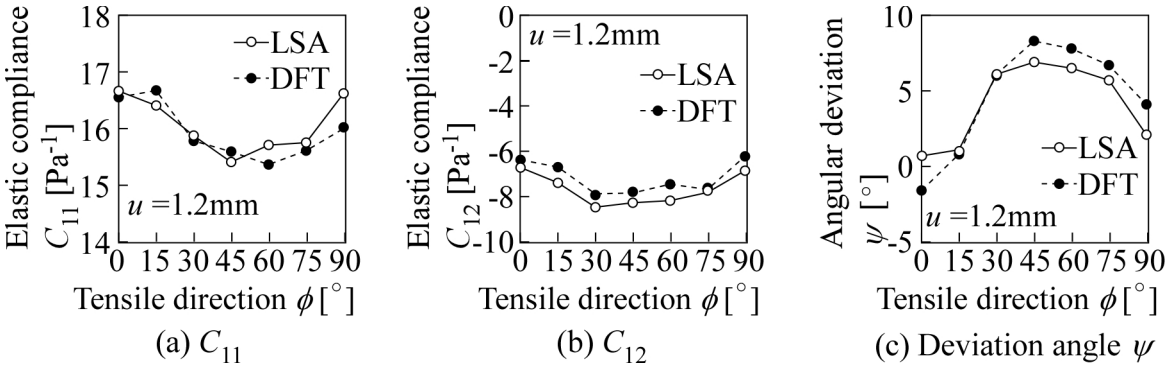

Figure 9 Variations in elastic compliances C_{11} and C_{12}, and deviation angle ψ with ϕ.

C_{12} did not vary significant, and its value ranged from -6 to -9 Pa^{-1}. Meanwhile, its planar anisotropy was similar to that of C_{11}, and the highest value was recorded at $\phi = 0°$ and $\phi = 90°$. Although a slight deviation was indicated between the two approximations, the effect was insignificant. The angle deviation shown in Fig. 9(c) was almost 0° at $\phi = 0°$ and $\phi = 90°$, where one of the structural symmetric axes was assumed to be in the tensile direction. The planar anisotropy exhibited four-fold symmetry, and the largest deviation of approximately 8° was indicated at $\phi = 90°$. As mentioned previously, this deviation, although small in magnitude, should be regarded as a significant deviation. The value estimated via the DFT was slightly larger than that estimated using LSA; however, the difference was not significant.

Plastic properties and deviation between principal axes of stress and strain

Fig. 10 shows the variations in plastic strains in the length and width directions and the angle deviation between the principal axes of stress and strain with increasing stroke under a tensile direction of 75°. Based on this figure, the results obtained from the two approximations are compared. In Fig. 10(a), the variations in plastic strain in the length direction, i.e., the tensile direction, are compared. As shown, the plastic strain increased linearly with the stroke between the chucks. Meanwhile, the plastic strain in the width direction decreased linearly as the stroke increased, as shown in Fig. 10(b). In both cases, almost no difference was observed between the results obtained using the two approximation methods. However, as shown in Fig. 10(c), the angle deviation increased significantly in the early stage by u = 1 mm. This suggests rotation in the

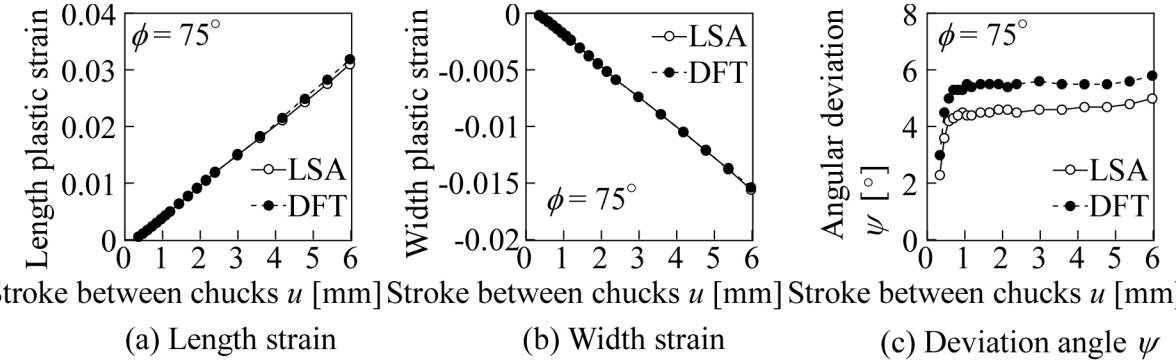

Figure 10 Variations in length and width plastic strains and deviation angle ψ for ϕ =75°.

principal axis of the plastic strain from the tensile direction to a certain stationary direction.

After the direction of the principal axis of the plastic strain became stationary, the angle deviation increased only slightly from 4° to 6°. Such a difference in the principal direction between

the stress and strain naturally generates shear strain in the tensile direction, and the strains in the tensile and vertical directions are no longer the principal values. In this case, the Lankford value evaluated via the ordinary method is not the ratio between the principal strains. In addition, an increase in the angular deviation in the early stage indicates that the deformation pattern varied continuously within a stroke of 1 mm. One can assume that such transitions in the deformation state occur consistently in the early stages after the stress state changes. The difference between the results yielded by the LSA and DFT ranged from 1° to 2°, which was considered insignificant.

The representative plastic properties include the planar strain ratio β and Lankford value r. They are defined as

$$\beta = \frac{\varepsilon_{\mathrm{p}}(90°)}{\varepsilon_{\mathrm{p}}(0°)}, \quad r = -\frac{\varepsilon_{\mathrm{p}}(90°)}{\varepsilon_{\mathrm{p}}(0°) + \varepsilon_{\mathrm{p}}(90°)}. \tag{5}$$

The planar anisotropies of the planar strain ratio, the Lankford value, and the angular deviation between the principal axes of stress and strain at u = 1.2 mm are shown in Fig. 11. Although the shape of the symmetry was not particularly neat, the planar anisotropy of the planar strain ratio exhibited four-fold symmetry, as shown in Fig. 11(a). Similar to the case of C_{11}, the highest value was indicated at ϕ = 0° and ϕ = 90°, and the lowest value near ϕ = 45°. The value of β was approximately 0.5 in a wide range, which implies that an almost isotropic deformation occurred within the range. The results obtained from the two approximations differed only slightly.

As shown in Fig. 11(b), the Lankfold value was inversely proportional to the planar strain ratio. This tendency was as expected, and the lowest value was approximately 0.7 at ϕ = 0° and ϕ = 90°, and the maximum value was 1.2 near ϕ = 45°. The angle deviation was approximately 0 at ϕ = 0° and ϕ = 90°, as expected. The planar anisotropy was similar to the four-fold symmetry, i.e. similar to Mohr's circle of elastic strain. The maximum deviation was approximately 6° and was indicated near ϕ = 45°, as similarly observed for the elastic strain in Fig. 9.

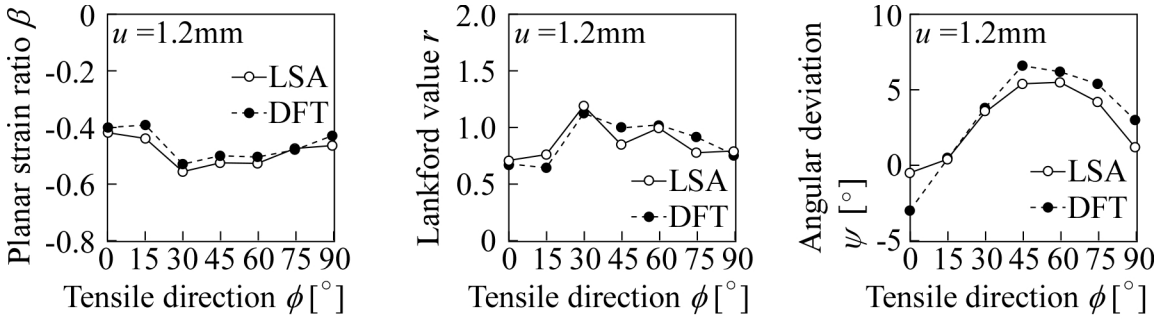

Figure 11 Variations in plastic strain ratios β and r, and deviation angle ψ with ϕ.

Correlations between elastic properties and plastic properties

Here, the correlations between elastic and plastic properties are discussed. First, the angle deviations obtained from Figs. 9(c) and 11(c) are compared in Fig. 12. In this figure, the angular deviation between the principal axes of the stress and plastic strain increments is shown as well. The plastic strain increment was calculated using the plastic strain results. As shown in this figure, the planar anisotropies of the angle deviation were similar those with four-fold symmetry. The value differed only slightly by 1° to 2° and thus exerted minimal effects. This indicates that the directions of the principal axes were identical for the three strains.

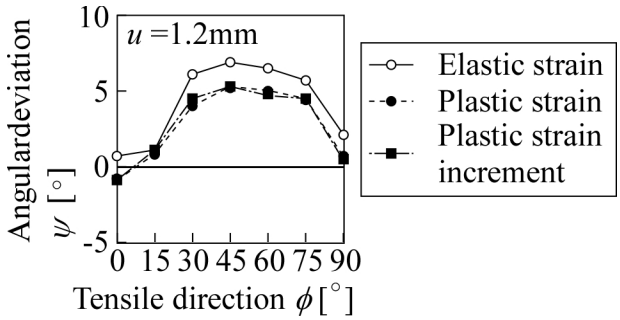

Fig. 12 Comparison of deviation angle ψ during elastic and plastic strains (LSA).

Finally, the undecided elastic compliance, C_{13}, was estimated from the previously obtained elastic and plastic properties. If the associated flow rule and coaxiality between the elastic-strain deviation and plastic strain can be assumed simultaneously, then C_{13} can be calculated. Here, if the elastic-strain deviation is expressed as the ordinary relation, then the relationship

$$C_{13} = 3\frac{C_{12} - \beta C_{11}}{1-\beta} - C_{11} - C_{12} \tag{6}$$

can be established. Based on the relationship above, the planar anisotropy of C_{13} for u = 1.2 mm was calculated using the results of the two approximations, and the results are shown in Fig. 13. As shown in this figure, the planar anisotropy of C_{13} showed four-fold symmetry as expected, and the maximum value was indicated near ϕ = 45°. The value was similar to that of C_{12}, and the variation in the direction was insignificant. No significant differences were observed between the two approximations.

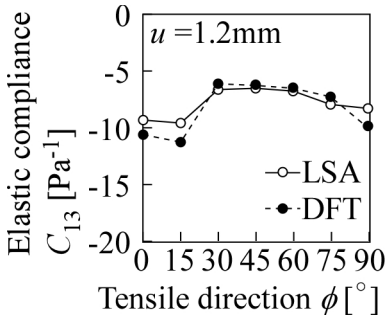

Fig. 13 Estimation of elastic compliance C_{13} from plastic strain ratio.

Conclusions

In this study, an incremental tensile test was conducted using eight strain gauges, and the variation in Mohr's strain circle with elongation was investigated to determine the elastic and plastic properties. For the elastic properties, both C_{11} and C_{12} as well as the angle deviation showed four-fold symmetry; meanwhile, the elastic compliances and angle deviation showed the minimum and the maximum values near the 45° direction from the rolling direction, respectively. The largest angle deviation was approximately 8°, which was not large but sufficiently significant. Similarly, the planar strain ratio and Lankford value showed four-fold symmetry as well as contrary tendencies. The planar anisotropy of the Lankford value was that typically observed. The angular deviation between the principal axes of stress and plastic strain showed four-fold symmetry, with a maximum value of approximately 6°. Almost no differences were observed between the two approximations. The direction of the principal strain can be regarded as identical for all elastic,

plastic, and plastic strain increments. Finally, the undecided elastic compliance C_{13} was estimated using the results for both the elastic and plastic properties.

Acknowledgement
This study was funded by the Amada Foundation (AF-2023055-X1). We are grateful for the support provided.

References

[1] J.F.W. Bishop, R. Hill, A theory of the Plastic Distortion of a Polycrystalline Aggregate under Combined Stresses, Phil. Mag. 42 (1951) 414-427. https://doi.org/10.1080/14786445108561065

[2] W.F. Hosfold, A Generalized Isotropic Yield Criterion, J. Appl. Mech. 39 (1972) 607-609. https://doi.org/10.1115/1.3422732

Reference to a chapter in an edited book:

[3] R. Hill, A theory of the yielding and plastic flow of Anisotropic Metals, Proc. Royal Soc. London A193 (1948) 281-297. https://doi.org/10.1098/rspa.1948.0045

[4] F. Barlat, D.J. Lege, J.C. Brem: A Six-component Yield Function for Anisotropic Materials, Int. J. Plast. 7 (1991) 693-712. https://doi.org/10.1016/0749-6419(91)90052-Z

[5] F. Barlat, R.C. Becker, Y. Hayashida, Y. Maeda, M. Yanagawa, K. Chung, J.C. Brem, D.J. Lege, K. Marsui, S.J. Murtha, S. Hattori, Yielding Description for Solution Strengthened Aluminum Alloys, Int. J. Plast. 13 (1997) 385-401. https://doi.org/10.1016/S0749-6419(97)80005-8

[6] F. Barlat, Y. Maeda, K. Chung, M. Yanagawa, J.C. Brem, Y. Hayashida, D.J. Lege, K. Matsui, S.J. Murtha, S. Hattori, R.C. Becker, S. Makosey, Yield Function Development for Aluminum Alloy Sheets, J. Mech. Phys. Solids 45 (1997) 1727-1763. https://doi.org/10.1016/S0022-5096(97)00034-3

[7] F. Barlat, J.C. Brem, J.W. Yoon, K. Chung, R.E. Dick, D.J. Lege, F. Pourboghrat, S.-H. Choi, E. Chu, Plane Stress Yield Function for Aluminum Alloy Sheets -Part I:Theory, Int. J. Plast. 19 (2003) 1297-1319. https://doi.org/10.1016/S0749-6419(02)00019-0

[8] J.F.W. Bishop, R. Hill, A Theoretical Derivation of the Plastic Properties of a Polycrystalline Face-centred Metal, Phil. Mag. 42 (1951) 1298-1397. https://doi.org/10.1080/14786444108561385

[9] J.W. Hutchinson, Plastic Stress-strain Relations of F.C.C Polycrystalline Metals Hardening According to Taylor's Rule, J. Mech. Phy. Solids 12 (1963) 11-24. https://doi.org/10.1016/0022-5096(64)90003-1

[10] R.W. Logan, W.F. Hosford, Upper-bound Anisotropic Yield Locus Calculations Assuming <111>-pencil Glide, Int. J. Mech. Sci. 22 (1980) 419-430. https://doi.org/10.1016/0020-7403(80)90011-9

[11] R.J. Asaro, Micromechanics of Crystals and Polycrystals, Adv. Appl. Mech. 23 (1983) 1-115. https://doi.org/10.1016/S0065-2156(08)70242-4